Chapter 13
Silicon Quantum Dots: From Synthesis to Bioapplications

Miruna Silvia Stan, Cornelia Sima and Anca Dinischiotu

Abstract Silicon quantum dots (Si QDs) represent a special class of nanomaterials with distinctive properties, being used in different applications such as photovoltaics, optoelectronics devices, and biomedical ones. They have excellent luminescence at UV irradiation, tunable band gap, and resistance against photobleaching compared to standard dyes. Being less toxic in comparison with conventional metal-containing QDs, they received growing research interest in the last decade as a more biocompatible alternative to which displayed toxicological concerns. There are several physical and chemical methods for Si QDs synthesis, each of them involving advantages and disadvantages. In physical methods, the experimental setup is very simple and parameters can be adjusted from outside in order to obtain the desired size of nanoparticles. Chemical methods seem to be attractive due to the huge scale of productions, but the purity control of the material and experimental setup are more complicated. For biomedical applications, many techniques have been established to achieve water-soluble Si QDs and for their conjugation with biomolecules that render them to specific biological targets. Si QDs have become powerful nanomaterials in various biomedical applications, a promising approach for in vivo imaging, tumor biology investigation, and cancer treatment. Besides of all these advantages, their characteristics can also trigger cytotoxicity in healthy cells by different mechanisms that have been in vitro and in vivo investigated in the last years. This chapter summarizes the major methods of synthesis and recent advances in bioconjugation strategies for preparing high-quality Si QDs, with a focus on their toxicity evaluation and bioapplications.

Keywords Silicon quantum dots · Semiconductors · Self-fluorescence · Biocompatibility · Biomedical applications

M.S. Stan · A. Dinischiotu (✉)
Department of Biochemistry and Molecular Biology, University of Bucharest, 91-95 Splaiul Independentei, 050095 Bucharest, Romania
e-mail: anca.dinischiotu@bio.unibuc.ro

C. Sima
Laser Department, National Institute of Laser, Plasma and Radiation Physics, 409 Atomistilor, 077125 Bucharest, Magurele, Romania

B. Yan et al. (eds.), *Bioactivity of Engineered Nanoparticles*, Nanomedicine and Nanotoxicology, DOI 10.1007/978-981-10-5864-6_13

13.1 Si QDs Synthesis

13.1.1 Quantum Dots Versus Organic Dyes

Silicon is a chemical element widely used in many industrial and biomedical applications. Compared with other semiconductor materials, silicon is found in a large quantity in the earth's crust. Although it is an indirect band-gap semiconductor material, in the bulk form is less used for optoelectronics and biological applications. However, by decreasing the size of the particles (usually less than 5 nm), silicon acquires special properties exhibiting luminescence due to the existence of quantum confinement effect [1–5]. Several parameters influence the quantum confinement, such as particle size and size distribution, particle density, and surface properties [6, 7].

Crystalline silicon nanoparticles show emission from infrared to blue when their size is less than 5 nm meaning an increasing of the band gap: blue (2.64–3.0 eV), green (2.25 eV), orange (2.05 eV), red (1.70–1.80 eV) and infrared (1.2–1.6 eV) [8, 9]. It is assumed that the quantum confined effect appears in quantum dots (QDs) when their size becomes comparable with the exciton Bohr radius (4 nm for silicon) [9–11].

Wei-Wi et al. [12] noticed that photoluminescence of silicon quantum dots (Si QDs) at room temperature, in an atmosphere type dependent manner. So in hydrogen or in a vacuum, the emission was from infrared to ultraviolet with a blue shift observed with the decreasing of nanocrystal size, whereas in oxygen, air or nitrogen a stronger emission in a narrower wavelength range occurred [12].

Over the years, several semiconductor QDs were studied: CdS, CdSe, CdTe, InP, InAs, GaAs, and PbSe, PbS. One of the main disadvantages of these standard QDs is that they use heavy metal elements and are not suitable for in vivo applications being very toxic for biological systems [1].

In order to surpass these drawbacks, extensive researches were developed to synthesize reliable QDs with less toxicity, for use in optoelectronic and bioimaging applications [13–15]. In this context, silicon proved to be one of the ideal candidates having significant advantages over standard QDs (PbS(Se) and CdSe(Te)): less toxic, increased photostability, emission in near infrared range, and not at least their compatibility with biological medium [14, 16].

In the biological experiments, conventional fluorophores used are organic substances composed of either chemically synthesized fluorescent dyes or genetically encoded fluorescent proteins that have some limitations such as short fluorescence duration, narrow excitation, and broad bandwidth emission [17]. In contrast, QDs have broad absorption and at the same time a narrow wavelength-tunable emission peak. The molar absorption coefficients are larger than 100,000,000 M^{-1} cm^{-1} at the excitation peak wavelength compared to organic fluorophores which is less than 250,000 M^{-1} cm^{-1} [1]. Additionally, the emission peak of QDs is also tunable by varying size of the particles, which is not possible for organic dyes that have often the emission bands unsymmetrical [1–4]. Moreover, the quantum yield of QDs is

high, in the range of 60–80%, in visible and near infrared domains, whereas in the case of organic dye it is less than 20% in the near infrared region [1].

The fluorescence lifetime of the Si QDs is longer (tens of ns or μs), while in the case of organic dye it is shorter (5 ns in the visible region and 1 ns in the near infrared) [1, 4]. On the other hand, it was shown that "short fluorescence lifetime in Si QDs is often associated with core-related recombination and longer lifetime is due to the existence of ultrafast trapping of excited carriers in surface states, preventing core recombination" [1].

The emission properties of QDs are dependent on the particle size, morphology, composition, surface architecture, as well as shell ligands.

In consequence, QDs are more convenient than conventional dye for bioimaging applications due to strong stability to photobleaching, high quantum yield, broad absorption profile, and size-tunable emission [18–20].

13.1.2 Physical, Morpho-Structural, Optical and Surface Properties

QDs are semiconductor nanocrystals with size smaller than the exciton Bohr radius that present quantum size effect [1, 11, 13, 21]. They present special and unique properties due to quantum confinement phenomenon [20]. More exactly, the quantum confinement in the case of QDs consists of limitation of few electrons inside of a semiconductor that when are excited, emit a light with a specific wavelength which depends on the dot size [22].

It is well known that silicon has a very weak absorption in the visible range due to its indirect band gap. As a result of the quantum confinement phenomenon, optical band gap of the QDs can be adjusted as a function of size [14]. They have wavelength-tunable visible light emission, which depends on the core size of the nanoparticles [23].

There are many studies concerning the photoluminescence properties, on the nanoparticles size and size distribution, surface functionalization (surface passivation), crystallinity, shape of the nanoparticles, temperature, aging, etc. [21].

Studies regarding the variation of photoluminescence depending on the nanoparticle size revealed that larger nanoparticles (8 nm) exhibited luminescence toward longer wavelengths while those with size about 2 nm presented luminescence at higher energy (blue region) [24, 25].

The advantage of the Si QDs compared to other materials is mainly due to the low toxicity of silicon and possibility of modifying the nanoparticle size in a wide range [26, 27]. Other characteristics such as rates of radiative recombination, lifetimes, and quantum efficiency strongly depend also on the size of QDs.

In the synthesis process, nature of *the ambient gas* had a strong influence on the crystallization state. Due to this fact, Si QDs grown in NH_3 with plasma enhanced chemical vapor deposition (PECVD) had a crystalline structure, whereas those

synthesized in N_2 gas were amorphous, suggesting that hydrogen present in gaseous NH_3 favored the crystallinity [28]. Analyzing the photoluminescence intensity of Si QDs prepared in SiH_4/N_2, it was observed that the highest intensity was noticed for those prepared in SiH_4/NH_3, and the lowest was observed in the case of the ones prepared in SiH_4/N_2, probably due to the effect of hydrogen passivation on reducing dangling bonds and nonradiative species [28, 29]. The decrease of size by increasing of N_2 flow rate resulted in an enhancement of quantum confinement and appearance of a blue shift [30, 31].

A clear dependence between band gap, size, and shape of QDs was reported [32]. Also, it was demonstrated that "cubic Si QDs exhibit larger wavelengths while octahedral nanoparticles exhibit smaller wavelengths and truncated Si QDs exhibit wavelengths between cubic and octahedral" [32]. It was also proved that plasma-based methods produced cubic shapes which are advantageous for "maximization of amount surface hydrogen absorption" while the other synthesis methods generated pseudospherical shapes which, after annealing, leaded to faceted shapes [32].

In the chemical etching synthesis method, the *etching time* also influences the photoluminescence; therefore, increasing the etching time, reduces the size of nanoparticles leading to a blue shifting in the photoluminescence peak [33].

Previous studies revealed that Si QDs with average size of about 3.6 nm did not present any photoluminescence immediately after synthesis. But, after about 20 min in air, they exhibited a weak photoluminescence at about 1.72 eV; by increasing the aging time in air to 25 days, the photoluminescence peak was at about 1.87 eV. It was concluded that the photoluminescence peak shifted toward shorter wavelengths, in an oxidation time dependent manner, probably due to the decrease of the core size and the increase of the oxide layer [24]. Also, the full width at half maximum (FWHM) after 20 min of aging was about 0.23 eV, and increased to 0.31 eV after 25 days. After 1 month, the peak intensity increased by about 16 times [24]. After 6 months of aging in air after SiO_2 removal, the luminescence peak position did not change, but FWHM returned to approximately the same value before oxidation. Additionally, the intensity strongly increased by about 70-fold [24]. Similar observations have been done by Ledoux et al. [25].

One of the most important parameters which influences the photoluminescence are the *surface properties* of Si QDs as well. Absence of a semiconductor shell reduces the degree of exciton confinement in the core and broadnesses the emission peak. It was demonstrated that Si QDs prepared via colloidal solution method have emission in blue–green while the red emission could be observed when Si QDs are prepared at high temperature. Also the crystallinity and size of the core of Si QDs are influenced by the oxidation of dots; therefore, by adding an organic monolayer on the Si QDs surface, oxidation of the surface could be avoided leading to stable photoluminescence properties [1].

Taking into account that surface of Si QDs is very active, several ways to modify the surface properties for improvement of the photoluminescence were studied [34]. So the surface of Si QDs (4.9–6 nm) was covered with an oxide layer by gradual

oxidation for 2 years in the air. After dispersion in ethanol, they exhibited a luminescence at about 763 nm, while the freshly prepared QDs had no photoluminescence [34].

It was assumed that the presence of dangling bonds on the silicon surface is a disadvantage for the photoluminescence occurrence and a passivation of Si QDs surface by hydrofluoric acid (HF) has been done in order to remove the oxide layer leading to a narrow band from 0.4 eV (before HF treatment) to 0.26 eV (after HF treatment) [35].

It was demonstrated that the dangling bonds (nonradiative defect) could be passivated using NH_3 instead of N_2. Furthermore, photoluminescence was very strong and the peak position was strongly influenced by the flow rate of NH_3 being shifted to lower wavelengths (blue shift) when the flow gas rate increased from 10 to 900 sccm at a fixed SiH_4 flow rate of 400 sccm. On the other hand, when the NH_3 flow rate was maintained at 30 sccm and SiH_4 flow rate was varied in the range 100–900 sccm, the photoluminescence peak shifted toward longer wavelengths [28].

When the Si QDs were capped with SH, NH_2, OH, photoluminescence spectra presented significant modifications, whereas when alky groups (–Si–C–) were added low alterations appeared in the photoluminescence spectrum [36].

The halogenation of the Si QDs strongly influenced the optical properties of QDs. So under direct UV irradiation of the halide attached on the Si QDs, no any photoluminescence was detected; but after oxidation it was noticed. Therefore, a blue photoluminescence was observed in the case of chlorine terminated silicon quantum dots surface, while for bromide and iodide, yellow–orange photoluminescence was observed. It was assumed that blue photoluminescence is due to oxychloride defects while the yellow orange is generated by oxide defects [37].

The photoluminescence of Si QDs is also influenced by *temperature.* A shifting toward red after an increase of temperature between 110 and 350 K, when the silicon sample was excited with 266 nm wavelength occurred [38]. Also after heating from 700 to 1000 °C the photoluminescence peak was shifted toward longer wavelengths due to the fact of the increase of the grain size at high temperatures [39].

The optical properties of the Si QDs are dependent on their *electronic structure* [40]. Theoretically, a strong correlation between the split of the energy level in the dot and the dot size, crystallographic directions, and shape exist [40]. Therefore, Zianni et al. [40] assumed that "for [001] level, the lifetime is not influenced by the crystallographic direction" and in the case of small dots (2 nm), it is of μs order while "for [100] level the lifetime is strongly influenced by the crystallographic direction" being about ms order [40].

It is considered that the photoluminescence lifetime is a result of radiative and nonradiative recombination processes. The study of Wu and Lin [41] on Si QDs revealed that "non-radiative recombination rate is much lower than radiative recombination rate," that means that the photoluminescence lifetime of these is the result of radiative recombination only [41].

13.1.3 Synthesis Methods

The synthesis methods of Si QDs are various being both physical and chemical ones. Each of them has advantages and disadvantages.

Physical methods produce high purity particles, the experimental setup being very simple and parameters can be adjusted from outside in order to obtain the desired size of nanoparticles; on the other hand, the particles have a lower yield [4].

Chemical methods seem to be attractive due to the huge scale of production, but the purity control of the material and experimental setup are more complicated. Unlike the physical methods, in order to enhance the QDs luminescence, additional treatment, such as annealing is necessary; moreover, multistep procedures are required [4].

There are several synthesis methods such as: laser ablation [6, 12, 26, 27, 42–52], magnetron sputtering [13, 53–55], solution phase oxidation/reduction [1, 4, 19, 56], thermolysis/laser pyrolysis [1, 4, 24, 25, 34, 35], electrochemical etching (anodic oxidation) [4, 5, 33, 38, 57, 58], microwave-assisted method [8, 11, 59–61], atmospheric pressure plasma [7, 62].

13.1.3.1 Laser Ablation

First experiments for preparing silicon nanoparticles by laser ablation have been done by Okada and Iijima [4, 42]. The method is advantageous due to the fact that no chemical precursors which could contaminate the nanoparticles is used (therefore, it is considered a very clean method); the experimental setup is very simple without the requirement of high temperatures or pressures; it is versatile, giving the possibility to vary from outside any experimental parameters [10].

There are two types of environments to prepare nanoparticles by laser ablation: in liquid or gas. Laser ablation in liquid demonstrated a good capability to produce pure nanoparticle colloidal solution. The photoluminescence of the silicon nanoparticles obtained in liquid is dependent of laser wavelength and pulse duration [43]. Intartaglia et al. [43] synthesized silicon nanoparticles in aqueous solution (deionized water) using a Ti: sapphire femtosecond laser, (110 fs pulse duration, 800 nm wavelength, 1 kHz repetition rate) at two different energies/pulse (0.15 and 0.4 mJ). In the case of high energy (0.4 mJ), the nanoparticles were in the range of 10–120 nm with an average size of about 65 nm. On the other hand, at low energy of 0.15 mJ, the size of the silicon nanoparticles was in the range of 1–8 nm with average size of about 5.5 nm. In both cases, the nanoparticles were crystalline. After synthesis, they were excited with 400 nm wavelength; the small nanoparticles (obtained at low energy) exhibited a blue green emission; the large ones (synthesized at high energy) exhibited a luminescence peak at 575 nm and decreased intensity [43].

Vaccaro et al. [44] evidenced also the versatility of the laser ablation in water, offering the possibility to control each parameter during the experiments

(wavelength, energy, fluency, pulse duration, liquid) leading to the desired properties of the silicon nanoparticles (crystallinity, composition, size). A nanosecond Nd:YAG laser (1064 nm, 10 Hz, 5 ns, 0.6 J/cm^2 energy density) was used. The nanoparticles were in the range of 2–10 nm with the mean size of about 4 nm. Concerning the photoluminescence, it was observed an emission peak at about 1.95 eV, being in accordance with quantum confinement. Therefore, decreasing the size of nanoparticle, the emission peak is shifted toward shorter wavelength and increasing the band gap. The measured photoluminescence lifetime was in the range of μs. It was demonstrated that the photoluminescence peak depends on the size of nanoparticle according to expression:

$$E_{\mathrm{PL}} = E_0 + \left(3.73/d^{1.39}\right), \tag{13.1}$$

where E_0 = 1.17 eV (the band gap energy of bulk silicon) and d = size of nanoparticle in nm [44].

Starting from a *p*-type silicon wafer, with a nanosecond Nd:YAG laser (532 nm, 13 ns, 10 Hz), Chewchinda et al. [45] synthesized silicon nanoparticles in ethanol, energy density from 0.15 to 0.45 J/cm^2. The nanoparticles were spherical, and their size was in the range of 2–30 nm, the average size decreasing with increasing of energy density. So at highest energy density of 0.45 J/cm^2, the average size was about 6 nm. In this case, the photoluminescence peak increases with increasing the energy density when small nanoparticles are generated and at the same time are blue shifted [45].

Eroshova et al. [26] studied the influence of the pulse duration on the nanoparticle characteristics. So, a picosecond laser (Nd:YAG, 1064 nm, 34 ps, 10 Hz, 1 mJ) was used for the ablation of a silicon wafer in distilled deionized water and femtosecond laser (1250 nm, 120 fs, 10 Hz, 300 μJ) in liquid nitrogen. The average size of nanoparticles obtained using picosecond laser was about 18 nm and these were crystalline. On the other hand, using fs laser for ablation in liquid nitrogen, the average size of the silicon nanoparticles was about 5 nm. In this case, the photoluminescence spectrum exhibited an emission peak at about 750 nm (1.65 eV).

Concerning the synthesis of Si QDs in a gas atmosphere, it was studied the temperature dependence of these nanoparticles produced by laser ablation in helium atmosphere [46]. Using a Nd:YAG laser (532 nm, 210 mJ, 10 Hz) a silicon wafer target was irradiated in an atmosphere of 7 Torr. Spherical nanoparticles with a very narrow lognormal distribution (6–8 nm) and average size about 7 nm were obtained. Additionally, it was observed that the silicon nanoparticles were covered with an amorphous silicon oxide shell due to the oxidation after exposure to the ambient atmosphere. From the photoluminescence spectra measured at different temperatures from 300 to 4 K, Orii et al. observed a "gradually increasing of the luminescence intensity, peaked at about 60 K and then decreasing rapidly. The photoluminescence intensity at 60 K was increased relative to the value of 300 K by a factor of 5 and that at 4 K decreased roughly to the value at 300 K" [46].

Another study used a KrF excimer laser (248 nm, 20 ns, 2 J/cm^2 fluency, 10 Hz), starting from a silicon target. The experiments were made in helium atmosphere at 10^{-1} mbar. All the silicon samples were almost spherical. The mean size of the nanoparticles was in the range of 1–5 nm. At room temperature, a UV–VIS photoluminescence attributed to direct band recombination from quantum confinement of silicon was observed. The photoluminescence lifetime was about 1.5 ns [6].

Laser ablation experiments in two different inert gases (helium and argon with pressure in the range of 250–550 mbar) were also made by Grigoriu et al. [47, 48]. A Nd:YAG laser (532/355 nm, 5 ns, 10 Hz and 4–8 J/cm^2) was used.

The synthesis of Si QDs by laser ablation in reactive gases was also done in oxygen atmosphere, using a KrF excimer laser (248 nm, 17 ns, 20 Hz, 5 J/cm^2) [49]. It was observed a strong dependence of the photoluminescence intensity on oxygen pressure and size of crystals. It was observed that increasing the oxygen pressure leads to a decreasing of the intensity photoluminescence. Additionally, the position and shape of the photoluminescence spectrum depend on the crystal size and size distribution; the crystal size decreases with increasing of oxygen pressure [49].

Wei-Qi et al. prepared Si QDs using infrared radiation, 1064 nm, 60–80 ns pulse duration, and 1000–3000 s^{-1} repetition rate [12]. They prepared Si QDs in different atmospheres: oxygen, nitrogen, air. A *p*-type silicon wafer was used as target. After synthesis, the samples were annealed at 1000 °C for 5–30 min in oxygen, nitrogen or air, in order to eliminate dangling bonds from the surface of Si QDs; the annealing produced a narrowing of the size range. Another method to reduce the dangling bonds was "the passivation of hydrogen in HF liquid" [12].

Concerning the correlation between pulse duration and nanoparticle characteristics, it is considered that laser ablation with picosecond pulses is more advantageous in comparison with nanosecond laser pulses. Therefore, when a laser with nanosecond pulse duration impinges the target, due to the high energies/pulse and low repetition rates, the ejected macroparticles interact with the gas leading to the formation of large particles. Conversely, using picosecond pulses, low energies/pulse and high repetition rates, a fine material is ejected from the target creating particles with small size [50].

13.1.3.2 Magnetron Sputtering

The method consists of bombardment of a target with energetic ions that come from gaseous plasma. Following the interaction between the ions and the atoms from target surface, the individual atoms condensed onto a substrate [53]. The method is very fast, simple, with high productivity, being similar with laser technique. The shape and size of the particles depend on the "distance between magnetron and exit aperture" [54]. Also, the aggregation of the particles is dependent on the distance between magnetron and exit aperture, gas pressure, and time [54].

By this method, Fujioka et al. obtained Si QDs with mean diameter about 6.5 nm and a core structure of silicon with average size of about 2.5 nm. At excitation wavelength of 300 nm, the photoluminescent emission was at 414 nm [13].

Ohta et al. synthesized Si QDs with diameter about 3 nm exhibiting luminescence at 450 nm after irradiation with 360 nm wavelength [55]. Generally, use of QDs in biological environments requires their dipping in aqueous medium thus leads to aggregation of the nanoparticles. In order to avoid the interaction between particles, it was necessary to modify their surface. For biomedical applications, their surfaces were modified by allylamine and amphiphilic block copolymers that did not modify the photoluminescence emission peak [55].

13.1.3.3 Solution Phase Oxidation/Reduction

The first experiment using this method has been performed by Heath in 1992 [56]. This is a simple method due to the flexibility of choosing different reducing agents [4, 56]. Ghosh et al. described in 2014 the synthesis method as consisting of a "reduction of $SiCl_4$ and $RSiCl_3$ (where R could be hydrogen or octyl group) by sodium metal in a non-polar organic solvent at high temperature of 385 °C and pressure higher than 100 atmosphere" [4]. The obtained silicon nanoparticles were in the range between 5 nm and 3 μm with hexagonal shapes in trichlorosilane or about 5.5 nm in the presence of trichlorooctylsilane [4]. On the other hand, this method is considered disadvantageous due to the difficulty of controlling or adjusting the nanoparticle size.

13.1.3.4 Thermolysis/Laser Pyrolysis

This method generates freestanding nanoparticles and was first demonstrated by Cannon et al. in silane gas, using a CO_2 laser [1, 4]. It consists in dissociation of SiH_4 and nucleation of the silicon nanoparticles [4]. Several authors investigated the Si QDs produced by laser pyrolysis [24, 25, 34, 35]. Ledoux et al. explained the principle method as follows: "a conical nozzle is placed near the pyrolysis "flame" and the clusters and nanoparticles are extracted from the flow reactor" [25]. "They are skimmed into a low-pressure vacuum chamber and form a "molecular beam" of noninteracting clusters." "In this molecular beam, the cluster velocity is mass dependent; the smaller the particles, the faster they are; therefore, a rotating chopper synchronized with the pulsed pyrolysis laser, the size distribution of the clusters can be significantly narrowed" [25]. This method can produce high quantities comparing with other methods; by laser pyrolysis about 200 mg/h particles with size less than 3 nm could be obtained [34]. The disadvantage is that is more complicated to obtain pure QDs and not at least silane is very explosive and should be taken additionally adequate protections which generate other supplementary costs.

13.1.3.5 Electrochemical Etching/Anodic Oxidation

Generally, the method consists in dissolving of the material which is subjected for obtaining of nanoparticles using some acids, basis, or several chemical agents. It could use different semiconducting materials (in this case silicon), metals or glass. Thus, after the interaction between the material and the respective chemical agents, the target is corroded and finally the material is removed. In order to adjust the size of the nanoparticles, the etching time could be varied as well as the etching solutions. One can be concluded that the characteristics of the nanoparticles depend on these parameters. Examples of etching solution could be considered nitric acid (HNO_3) and hydrofluoric acid (HF) [58]. More exactly, silicon wafer is etched and the resulted materials are dispersed in different solvents leading to a suspension with Si QDs of irregular shapes, with size from few nm to microns [4]. Wang and his coworkers [5], synthesized photoluminescent (red–orange) silicon nanoparticles (about 2.7 nm size) by electrochemical etching, starting from a silicon *n*-type or *p*-type wafer. Both wafers were etched in a mixture of HF/H_2O/ethanol [5]. This method is a promising one but it should be mentioned that the size of nanoparticles cannot be easy controlled "at the single nanoscale" [4].

13.1.3.6 Microwave-Assisted Synthesis Method

One experimental setup for obtaining silicon nanoparticles is reported by Chinnathambi et al. [11]. The method is based on a heating mechanism being known as "microwave dielectric heating" [60]. Baretto et al. [59] and Atkins et al. [60] give some explanation of the synthesis method with their advantages as follows. The heating takes place through two processes: dipolar polarization and ionic conduction. Thus, after the electromagnetic field is applied to the sample, the electrical component produces "dipols and ions which try to align with the electric field." Procedure of the alignment of the dipols with electric field involves "energy which is lost as generation of heat" [60].

The microwave-assisted synthesis method proved to be advantageous being a very fast and simple method. So, 0.1 g Si QDs of 4 nm size are obtained in about 15 min [61]. These have shown excellent aqueous dispersibility and a strong fluorescence. The spherical shape, high crystallinity and average size of about 3.1 nm were obtained. The emission peak of Si QDs was at 660 nm. Under UV irradiation, it could be seen a very strong red luminescence [61].

13.1.3.7 Atmospheric Pressure Plasma

Synthesis of Si QDs by atmospheric pressure plasma is considered one recent method with high capabilities for different applications.

An experimental setup of synthesis of Si QDs by plasma was described by Yu et al. [62]. Between two parallel aluminum electrodes covered with quartz as

dielectric barrier vertically in the reaction chamber, plasma was generated. As working gases, argon, silane, and hydrogen flow through the electrodes conducted at a discharge. Thus, the electrons from plasma dissociate the silane resulting into silicon clusters and after about several milliseconds generated few nanometers particles which were collected onto a substrate when an RF power is attached. The photoluminescence of the nanoparticles remain unchanged more than 1 month [62].

One of the main drawbacks of this method is that it takes long time for obtaining important quantities. The aim is to have a continuous flow-through process; therefore it was demonstrated that RF frequencies were more suitable from production rate point of view, comparing with DC excitation [7].

13.2 Si QDs Bio-Interaction

13.2.1 Si QDs Biocompatibility and Cytotoxicity

As stated before, Si QDs have proved an increased in vitro biocompatibility and low cytotoxicity, or even the absence of it [61, 63–66]. Compared with the heavy metal-based QDs, the toxicity of Si QDs was not observed at 112 μg/ml, and these proved to be more than ten times safer than CdSe QDs [13]. Despite the biocompatibility observed for low doses of nanoparticles, a reduced viability was noticed when the concentration was increased in respect with the type of synthesis which certainly influences the toxicity [13, 61, 63, 67–70]. Erogbogbo et al. considered that residual chloroform used in synthesis could be responsible for the toxic effects. The mechanism of toxicity suggested by the group of Fujioka pointed out that Si QDs can generate reactive oxygen species (ROS) which could be associated with membrane damage [63]. Similar, Stan et al. revealed the absence of toxicity in human lung cells for doses up to 200 μg/ml after 24 h of exposure, but toxic effects appeared for high concentrations after 48 and 72 h [70]. Similarly, HepG2 hepatic cells tolerated high doses of Si QDs without suffering significant damage [71]. The negative influence of Si QDs on redox homeostasis of pulmonary fibroblasts was reflected by increased levels of ROS, lipid peroxidation and oxidized proteins, together with decreased glutathione content, the intracellular distribution of GSH being altered during longer incubation intervals [70]. Taking into account all these in vitro data, it could be suggested that cell death induced by high doses of Si QDs is mediated by oxidative stress, a common key factor involved in the cytotoxicity of various types of nanoparticles, which disturbs protein functions and cell signaling [72]. In addition, an inflammatory response in lung cells characterized by the release of pro-inflammatory cytokines was triggered by Si QDs which modulated also the expression and activity of matrix metalloproteinases [69]. A schematic representation of the most important effects induced by Si QDs is depicted in Fig. 13.1.

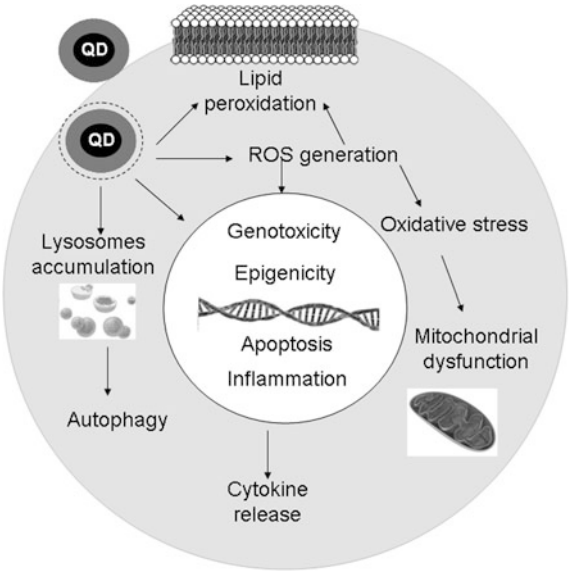

Fig. 13.1 A schematic representation of the most important effects induced by Si QDs

The surface chemistry of Si QDs can modulate their cytotoxicity, nanoparticles capped with polar molecules being less toxic than QDs with more relative functionalities [73]. In addition, our group considered that toxic effects of Si QDs could be related to the siloxane rings formed through the condensation of silanol groups which were expected to appear due to the hydroxylation of SiO_2 surface consecutively to laser ablation synthesis [69].

Studies over the past decade have shown that autophagy is part of the biological effects triggered by different nanoparticles, including QDs [69, 74], highlighting an increased expression of LC3-II and ATG7 proteins, and the possibility that autophagy could be triggered by the oxidized environment created after the exposure, and not directly by the nanoparticles [75]. Induction of autophagy could be seen as a cellular survival mechanism which allows self-clearance of nanoparticles which were frequently detected in lysosomes upon internalization, although their biopersistence could cause lysosomal disfunction [76]. Moreover, the degree of cellular uptake QDs might determine the cytotoxic potential.

The in vivo biocompatibility of Si QDs has been previously assessed especially to provide the confirmation for a future safety use in humans of these nanoparticles in biomedical applications [2, 77, 78]. The results obtained suggested that systemic reactions were specific to each type of model organism used and cytotoxicity appeared mostly at higher doses [77–83].

In addition, complex investigations were performed on gibel and crucian carp to establish the effects induced in fish on short and long terms because fish represent attractive alternative models to mammalian species for the analysis of toxicity mechanism induced by nanoparticles. Oxidative stress induced in fish liver by Si QDs was revealed 1-week post-administration [80]. Further, the profile of oxidative

stress markers and of heat shock proteins after 3 weeks post-injection indicated liver recovery after Si QDs-induced redox imbalance, suggesting that a longer period of time was necessary to overcome the harmful effects of QDs [81]. Besides degenerative processes, nephrogenesis was initiated after a week post-injection which indicated the ability of kidney to regenerate after the Si QDs-induced injury hallmarked by the increased lipid peroxidation and decreased level of reduced glutathione and of glutathione reductase and glutathione peroxidase activities [82]. Interestingly, an effective adaptative response was activated in the white muscle of gibel fish, and thus the oxidative stress induced by QDs did not cause any permanent damage in this tissue [83].

13.2.2 Si QDs Internalization and Accumulation

The typical pathway described for in vitro Si QDs uptake was endocytosis as reviewed by Cheng et al. [1]. Differences on the uptake rate were reported between normal and cancer cells, many more Si nanocrystals being found in the neoplastic cells after the internalization via cholesterol-dependent endocytosis [84]. Time course observations of Si QDs uptake revealed their transport to late endosomes/lysosomes, the number of internalized nanoparticles increasing with time and reaching a plateau value [69, 85]. Consequently, the removal of Si QDs from endothelial cells was reported via exocytosis, a kinetic model based on the mass balance of QDs and cell receptors being proposed [85]. Tu et al. showed a receptor-mediated accumulation of manganese-doped Si QDs in macrophages due to the dextran sulfate coating [68].

Although blue- and green-emitting Si QDs synthesized by atmospheric plasma method were visualized manly in the cytoplasm, along with a significant fraction inside the nucleus of the monocytes [2], our group observed the red-emitting Si QDs obtained by laser ablation only in the cytoplasm of lung fibroblasts [69]. These differences are most probably based on the QDs synthesis method, concentration and cellular type used in the experiments. Anyway, a concentration-dependent increase in LDH level and in the number of apoptotic and necrotic cells was noticed in both studies, underling the cytotoxicity of high doses of Si QDs.

Regarding the Si QDs accumulation in animals, studies showed the presence of high levels in liver and spleen of mice after three months of treatment investigated by Liu et al. [78]. However, these effects were not noticed in monkeys, suggesting that some systemic reactions could be dependent on the animal model [78]. A recent study on zebrafish model revealed a distribution of blue and green fluorescence of Si QDs mainly in the yolk-sac region, probably due to their interaction with lipid-rich yolk cells during embryonic development [2]. Although the authors stated that Si QDs induced a low toxicity in zebrafish, abnormalities, such as yolk-sac edema, head edema, and tail truncation, were observed, possibly due to a miss-regulation of certain genes, as it was noticed also for silver nanoparticles [2].

Furthermore, Tu et al. evaluated the biodistribution in mice of ^{64}Cu-DO3A derivative four labeled dextran-coated Si_{Mn} QDs (1% manganese-doped Si QDs) by in vivo positron emission tomography (PET) imaging [77]. The main sites of accumulation were urinary bladder and liver during the first hour after injection, and via gamma counting of ex vivo tissues after 48 h PET scan the liver was found to be the major organ where QDs accumulated. Regarding the nanoparticle excretion, it was demonstrated that the particles smaller than 7 nm are rapidly eliminated through renal filtration, and the larger ones are taken up by the reticuloendothelial system being excreted into the biliary system [77].

Tissue fluorescence microscopy revealed a gradual accumulation of Si QDs in gibel carp liver during the next 7 days post-injection which induced important histological changes in the hepatic tissue [80]. Also the presence of Si QDs in the liver of crucian carp was evidenced after 2 weeks post-administration and significantly disappeared after 3 weeks [81]. Regarding the biodistribution of Si QDs in the fish kidney, a progressive loading of renal tubular epithelial cells with nanoparticles was noticed along with their accumulation in the macrophages [82]. Visualization of Si QDs in the white skeletal muscle of gibel fish showed a localization pattern in the subsarcolemmal space and inside muscle fibers which generated degenerative changes [83].

13.3 Bioapplications of Si QDs

Their special optical properties make Si QDs a promising material for a large variety of applications ranging from optoelectronic devices, solar cells, energy storage materials to in vivo imaging labels, therapy, and contrast agents in bioimaging (Fig. 13.2). Due to their large emission in the infrared region are very useful for deep-tissue penetration [11, 20, 43]. Also, they can be used as photoluminescence probes in photodynamic diagnostics and therapy [26].

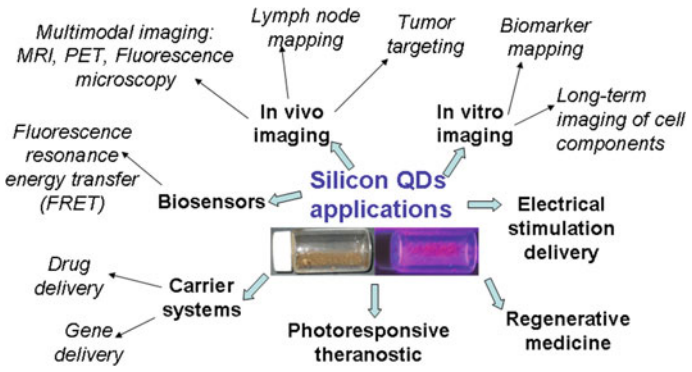

Fig. 13.2 The most important biomedical applications of Si QDs

It was proved that they could be used as drug and gene carriers for different treatments and imaging agents in magnetic resonance imaging (MRI), ultrasound (US), computed tomography (CT), photoacoustic (PA), and fluorescence imaging. For these applications, the particles should be nontoxic with increased photostability and highly resistant to the enzymatic degradation in physiological medium. Consequently, semiconductor QDs have been successfully demonstrated as in vitro and in vivo imaging probes in the field of medicine because they do not damage upon continuous light exposure [2, 45].

Since 2004 when Li and Ruckenstein [86] opened the research of Si QDs fluorescence imaging, several recent reports have illustrated the applicability of highly luminescent Si QDs as nontoxic in vitro and in vivo bioimaging probes. First, Erogbogbo et al. published in 2008 the preparation of biocompatible micelle-encapsulated Si QDs used for imaging pancreatic cancer cells [63]. Later on, water dispersible Si QDs of low toxicity coated with Pluronic F127 block copolymer were developed by Shen et al. for a long-term real-time observation of endoplasmic reticulum in live cells [64]. Other biocompatible and photostable Si QDs suitable for long-term imaging of cell nuclei for up to 60 min were described by Zhong et al. [65]. The use of Si QDs synthesized by one-step hydrothermal method as probes for fluorescent imaging was also illustrated by Wu et al. [66].

The excellent photophysical features of Si QDs have permitted the combination of their surface chemistry with optical microscopy in the context of bioimaging. Nanocrystalline Si QDs were used in fluorescence lifetime imaging microscopy (FLIM), which was successfully combined with Förster resonance energy transfer (FRET) studies where QDs revealed an enhanced performance as biosensors over conventional molecular fluorophores [18]. In this case, organic dye acceptors were conjugated onto the nanoparticle surface and contributed to the color tuning of nanoparticles [18]. Also, an energy transfer micelle platform was created in order to improve the QD emission yield for biological applications [67]. By combining Si QDs with an anthracene-based dye in the hydrophobic core of 1,2-distearoyl-sn-glycero-3-phosphoethanolamine-*N*-[methoxy(polyethylene glycol)-2000] (DSPE-PEG) micelles the luminescence was enhanced by more than 80% [67].

Nanostructured multimodal imaging probes can be achieved by combining the MRI technique and the optical imaging methods. Although Si QDs do not exhibit paramagnetic properties, the dual character can be obtain through their co-encapsulation with paramagnetic Fe_3O_4 nanoparticles in phospholipids [87], being doped with manganese [68] or by direct attachment of DOTA-chelated Gd^{3-} to the PEGylated micelles with hydrophobic Si QDs in their core [88], resulting a prolonged T1 relaxation time for an improved contrast while the fluorescence intensity was maintained. Also, Tu et al. demonstrated the efficiency of ^{64}Cu-DO3A derivative four labeled dextran-coated Si_{Mn} QDs (1% manganese-doped Si QDs) as a new biomedical candidate for in vivo positron emission tomography (PET) imaging [77]. Moreover, luminescent Si QDs functionalized with 2-vinylpyridine were developed by Klein et al. in 2009 as self-tracking vehicle for siRNA delivery in tumor cells. The biocompatible and water-soluble luminescent Si QDs were internalized by endocytosis, and the Si QDs-siRNA complexes formed via electrostatic interactions,

were internalized by endocytosis [89]. Prasad and his team succeeded to encapsulate Si QDs in Pluronic® block copolymers (PSiQDs). These were water dispersible, protected against oxidation and aggregation and with preserved optical properties [90]. Their surface modification with anti-claudin-4 and anti-mesothelin in order to target pancreatic cancer cells led to an improved uptake of these nanoconstructs compared to folate-conjugated PSiQDs, being competitive for tumor targeting in cancer applications without exhibiting toxicity. Moreover, the same group of Prasad developed a nanoplatform with both plasmonic and luminescent properties for multimodal imaging by incorporating multiple Si QDs into the core of a micelle and depositing plasmonic gold on its surface [91].

The potential of Si QDs as carriers in drug-delivery systems was evaluated after their conjugation with alminoprofen, a non-steroid anti-inflammatory drug for rheumatism [92]. The results revealed a lower toxicity of the "silicon drug" compared to the parental alminoprofen due to a condensed surface integration of ligand/receptor-type drugs which might reduce the adverse interaction between the cells and ligants, and also an enhanced functionality of the anti-inflammatory drug [92]. In addition, doxorubicin-loaded Si QD aggregates were designed for the intracellular release of drug in response to endosomal pH decrease [85]. Recently, a drug-delivery system based on amine functionalized Si QDs and covalently conjugated phototrigger *o*-nitrobenzyl with caged anticancer drug chlorambucil onto it, was designed as a photoresponsive theranostic which combines multiple functions [93]. Besides the nanocarrier role for drug delivery and the controlled drug release under one- and two-photon excitation, these photoswitchable fluorescent nanoparticles allowed the real-time monitoring of drug release based on the photoinduced electron transfer process [93].

The in vivo imaging using QDs was reported especially for lymph node mapping, blood vessel visualization, and tumor targeting. Si QDs with a hydrodynamic size of 20 nm, injected subcutaneously to mice were observed in the axillary lymph nodes and a long tumor accumulation time in vivo, without any important adverse effects which suggest their biocompatibility compared with cadmium containing QDs [79]. This opportunity to track the lymphatic flow in real time and to guide the nodal resection given by the noninvasive fluorescence detection of sentinel lymph nodes using QDs is very useful.

Recently, Erogbogbo and his coworkers managed to translate the metabolomic and proteomic data obtained in a human model of cardiac ischemia into a potential therapeutic diagnostic (theranostic) containing Si QDs. The fabrication of such theranostic nanoconstruct represents an important step which should be adopted in the pathway to a personalized medicine [94].

Besides fluorescence imaging and drug-delivery applications, the large variety of biomedical purposes of Si QDs includes also the regenerative medicine. In this way, the group of Olson has investigated the capability of intravitreal Si QDs to deliver electrical stimulation to the retinal cells and the effects on retinal electrophysiology and anatomy [95]. The use of Si QDs in the rat model of retinal photoreceptor degeneration was safe, providing a prolonged cell survival rate and increased

amplitude of the b-wave, mainly in the rod's response. This great opportunity of nanotechnology to deliver electrical stimulation at molecular level should represent a priority for future biomedical research on Si QDs to raise the cure rate of various diseases.

References

1. Cheng X, Lowe SB, Reece PJ, Gooding JJ (2014) Colloidal silicon quantum dots: from preparation to the modification of self-assembled monolayers (SAMs) for bio-applications. Chem Soc Rev 43:2680–2700
2. Fan JW, Vankayala R, Chang CL, Chang CH, Chiang CS, Hwang KC (2015) Preparation, cytotoxicity and in vivo bioimaging of highly luminescent water-soluble silicon quantum dots. Nanotechnology 26:215703
3. Alima D, Estrin Y, Rich DH, Bar I (2012) The structural and optical properties of supercontinuum emitting Si nanocrystals prepared by laser ablation in water. J Appl Phys 112:114312
4. Ghosh B, Shirahata N (2014) Colloidal silicon quantum dots: synthesis and luminescence tuning from the near-UV to the near-IR range. Sci Technol Adv Mater 15:014207
5. Hwang J, Jeong Y, Lee KH, Seo Y, Kim J, Hong JW, Kmaloo E, Camesano TA, Choi J (2015) Simple preparation of fluorescent silicon nanoparticles from used Si wafers. Ind Eng Chem Res 54:5982–5989
6. Chaturvedi A, Joshi MP, Rani E, Ingale A, Srivastava AK, Kukreja LM (2014) On red-shift of UV photoluminescence with decreasing size of silicon nanoparticles embedded in SiO_2 matrix grown by pulsed laser deposition. J Lumin 154:178–184
7. Askari S, Macias-Montero M, Velusamy T, Maguire P, Svrcek V, Mariotti D (2015) Silicon-based quantum dots: synthesis, surface and composition tuning with atmospheric pressure plasmas. J Phys D Appl Phys 48:314002
8. Gupta A, Wiggers H (2011) Freestanding silicon quantum dots: origin of red and blue luminescence. Nanotechnology 22:055707
9. Shcherbyna L, Torchynska T (2013) Si quantum dot structures and their applications. Physica E 51:65–70
10. Huan C, Shu-Qing S (2014) Silicon nanoparticles: preparation, properties, and applications. Chin Phys B 23:088102
11. Chinnathambi S, Chen S, Ganesan S, Hanagata N (2014) Silicon quantum dots for biological applications. Adv Healthc Mater 3:10–29
12. Huang WQ, Miao XJ, Huang ZM, Liu SR, Qin CJ (2012) Activation of silicon quantum dots for emission. Chin Phys B 21:094207
13. Fujioka K, Hiruoka M, Sato K, Manabe N, Miyasaka R, Hanada S, Hoshino A, Tilley RD, Manome Y, Hirakuri K, Yamamoto K (2008) Luminescent passive-oxidized silicon quantum dots as biological staining labels and their cytotoxicity effects at high concentration. Nanotechnology 19:415102
14. Zhou T, Anderson RT, Li H, Bell J, Yang Y, Gorman BP, Pylypenko S, Lusk MT, Sellinger A (2015) Bandgap tuning of silicon quantum dots by surface functionalization with conjugated organic groups. Nano Lett 15:3657–3663
15. Chatterjee S, Mukherjee TK (2013) Size-dependent differential interaction of allylamine-capped silicon quantum dots with surfactant assemblies studied using photoluminescence spectroscopy and imaging technique. J Phys Chem C 117:10799–10808
16. Joo J, Liu X, Kotamraju VR, Ruoslahti E, Nam Y, Sailor MJ (2015) Gated luminescence imaging of silicon nanoparticles. ACS Nano 9:6233–6241
17. Lee KH (2007) Quantum dots for molecular imaging. J Nucl Med 48:1408–1410

18. Cheng X, Hinde E, Owen DM, Lowe SB, Reece PJ, Gaus K, Gooding JJ (2015) Enhancing quantum dots for bioimaging using advanced surface chemistry and advanced optical microscopy: application to silicon quantum dots (SiQDs). Adv Mater 27:6144–6150
19. Wang Y, Wang H, Guo J, Wu J, Gao LJ, Sun YH, Zhao J, Zou GF (2015) Water-soluble silicon quantum dots with quasi-blue emission. Nanoscale Res Lett 10:300
20. Cheng X, Lowe SB, Ciampi S, Magenau A, Gaus K, Reece PJ, Gooding JJ (2014) Versatile "Click Chemistry" approach to functionalizing silicon quantum dots: applications toward fluorescent cellular imaging. Langmuir 30:5209–5216
21. Chen X, Yang P (2015) Preparation and photovoltaic properties of silicon quantum dots embedded in a dielectric matrix: a review. J Mater Sci Mater Electron 26:4604–4617
22. Barbadikar D, Gautam R, Sahare S, Patrikar R, Bhatt J (2013) Optimization of process parameter for synthesis of silicon quantum dots using low pressure chemical vapour deposition. Bull Mater Sci 36:483–490
23. DeBenedetti WJI, Chiu SK, Radlinger CM, Ellison RJ, Manhat BA, Zhang JZ, Shi J, Goforth AM (2015) Conversion from red to blue photoluminescence in alcohol dispersions of alkyl-capped silicon nanoparticles: insight into the origins of visible photoluminescence in colloidal nanocrystalline silicon. J Phys Chem C 119:9595–9608
24. Huisken F, Ledoux G, Guillois O, Reynaud C (2002) Light-emitting silicon nanocrystals from laser pyrolysis. Adv Mater 14:1861–1865
25. Ledoux G, Guillois O, Porterat D, Reynaud C (2000) Photoluminescence properties of silicon nanocrystals as a function of their size. Phys Rev B 62:15942–15951
26. Eroshova OI, Perminov PA, Zabotnov SV, Gongal'skii MB, Ezhov AA, Golovan LA, Kashkarov PK (2012) Structural properties of silicon nanoparticles formed by pulsed laser ablation in liquid media. Crystallogr Rep 57:831–835
27. Xin Y, Nishio K, Saitow K (2015) White-blue electroluminescence from a Si quantum dot hybrid light-emitting diode. Appl Phys Lett 106:201102
28. Kim BH, Cho CH, Kim TW, Park NM, Sung GY, Park SJ (2005) Photoluminescence of silicon quantum dots in silicon nitride grown by NH_3 and SiH_4. Appl Phys Lett 86:091908
29. Wu Q, Wang X, Li QS, Zhang RQ (2013) Excited state relaxation and stabilization of hydrogen terminated silicon quantum dots. J Clust Sci 24:381–397
30. Park NM, Kim SH, Sung GY, Park SJ (2002) Growth and size control of amorphous silicon quantum dots using SiH_4/N_2 plasma. Chem Vap Depos 8:254–256
31. Someno K, Usami K, Kodera T, Kawano Y, Hatano M, Oda S (2012) Photoluminescence of nanocrystalline silicon quantum dots with various sizes and various phosphorus doping concentrations prepared by very high frequency plasma. Jpn J Appl Phys 51:115202
32. Barnard AS, Wilson HF (2015) Optical emission of statistical distributions of silicon quantum dots. J Phys Chem C 119:7969–7977
33. Le TH, Jeong HD (2014) Characterization of band gaps of silicon quantum dots synthesized by etching silicon nanopowder with aqueous hydrofluoric acid and nitric acid. Bull Korean Chem Soc 35:1523–1528
34. Vincent J, Maurice V, Paquez X, Sublemontier O, Leconte Y, Guillois O, Reynaud C, Herlin-Boime N, Raccurt O, Tardif F (2010) Effect of water and UV passivation on the luminescence of suspensions of silicon quantum dots. J Nanopart Res 12:39–46
35. Ledoux G, Gong J, Huisken F (2001) Effect of passivation and aging on the photoluminescence of silicon nanocrystals. Appl Phys Lett 79:4028–4030
36. Li QS, Zhang RQ, Lee ST, Niehaus TA, Frauenheim T (2008) Optimal surface functionalization of silicon quantum dots. J Chem Phys 128:244714
37. Dasog M, Bader K, Veinot JGC (2015) Influence of halides on the optical properties of silicon quantum dots. Chem Mater 27:1153–1156
38. Amans D, Guillois O, Ledoux G, Porterat D, Reynaud C (2002) Influence of light intensity on the photoluminescence of silicon nanostructures. J Appl Phys 91:5334–5340
39. Kim BH, Davis RF, Park SJ (2010) Optical property of silicon quantum dots embedded in silicon nitride by thermal annealing. Thin Solid Films S18:1744–1746

40. Zianni X, Nassiopoulou AG (2006) Photoluminescence lifetimes of Si quantum dots. J Appl Phys 100:074312
41. Wu CL, Lin GR (2012) Inhomogeneous linewidth broadening and radiative lifetime dispersion of size dependent direct bandgap radiation in Si quantum dot. AIP Adv 2:042162
42. Okada R, Iijima S (1991) Oxidation property of silicon small particles. Appl Phys Lett 58:1662–1663
43. Intartaglia R, Bagga K, Scotto M, Diaspro A, Brandi F (2012) Luminescent silicon nanoparticles prepared by ultra short pulsed laser ablation in liquid for imaging applications. Opt Mater Express 2:510–518
44. Vaccaro L, Sciortino L, Messina F, Buscarino G, Agnello S, Cannas M (2014) Luminescent silicon nanocrystals produced by near-infrared nanosecond pulsed laser ablation in water. Appl Surf Sci 302:62–65
45. Chewchinda P, Odawara O, Wada H (2014) The effect of energy density on yield of silicon nanoparticles prepared by pulsed laser ablation in liquid. Appl Phys A 117:131–135
46. Orii T, Hirasawa M, Seto T, Aya N, Onari S (2003) Temperature dependence of photoluminescence from mono-dispersed Si nanoparticles. Eur Phys J D 24:119–122
47. Grigoriu C, Nicolae I, Ciupina V, Prodan G, Suematsu H, Yatsui K (2004) Influence of the experimental parameters on silicon nanoparticles produced by laser ablation. J Optoelectron Adv Mater 6:825–830
48. Grigoriu C, Kuroki Y, Nicolae I, Zhu X, Hirai M, Suematsu H, Takata M, Yatsui K (2005) Photo and cathodoluminescence of Si/SiO_2 nanoparticles produced by laser ablation. J Optoelectron Adv Mater 7:2979–2984
49. Riabinina D, Durand C, Chaker M, Rosei F (2006) Photoluminescent silicon nanocrystals synthesized by reactive laser ablation. Appl Phys Lett 88:073105
50. Wu MH, Mu R, Ueda A, Henderson DO, Vlahovic B (2005) Production of silicon quantum dots for photovoltaic applications by picosecond pulsed laser ablation. Mater Sci Eng B 116:273–277
51. Mahdieh MH, Momeni A (2015) From single pulse to double pulse ns laser ablation of silicon in water: photoluminescence enhancement of silicon nanocrystals. Laser Phys 25:015901
52. Nakamura T, Yuan Z, Adachi S (2014) High-yield preparation of blue emitting colloidal Si nanocrystals by selective laser ablation of porous silicon in liquid. Nanotechnology 25:275602
53. Kelly PJ, Arnell RD (2000) Magnetron sputtering; a review of recent developments and applications. Vacuum 56:159–172
54. Tang W, Eilers JJ, van Huis MA, Wang D, Schropp REI, Di Vece M (2015) Formation and photoluminescence of "cauliflower" silicon nanoparticles. J Phys Chem C 119:11042–11047
55. Ohta S, Shen P, Inasawa S, Yamaguchi Y (2012) Size- and surface chemistry-dependent intracellular localization of luminescent silicon quantum dot aggregates. J Mater Chem 22:10631–10638
56. Heath JR (1992) A liquid solution phase synthesis of crystalline silicon. Science 258:1131
57. Belomoin G, Therrien J, Smith A, Rao S, Twesten R (2002) Observation of a magic discrete family of ultrabright Si nanoparticles. Appl Phys Lett 80:841–843
58. Sato K, Tsuji H, Hirakuri K, Fukata N, Yamauki Y (2009) Controlled chemical etching for silicon nanocrystals with wavelength-tunable photoluminescence. Chem Commun 25:3759–3761
59. Baretto GP, Morales G, Lopez Qintanilla ML (2013) Microwave assisted synthesis of ZnO nanoparticles: effect of precursor reagents, temperature, irradiation time and additives on nano-ZnO morphology development. J Mater 2013. Article ID 478681
60. Atkins TM, Louie AY, Kanzlarich SM (2012) An efficient microwave-assisted synthesis method for the production of water soluble amine-terminated Si nanoparticles. Nanotechnology 23:294006
61. He Y, Zhong Y, Peng F, Wei X, Su Y, Lu Y, Su S, Gu W, Liao L, Lee ST (2011) One-pot microwave synthesis of water-dispersible, ultraphoto- and pH-stable, and highly fluorescent silicon quantum dots. J Am Chem Soc 133:14192–14195

62. Yu W, Xu Y, Li H, Zhan X, Lu W (2013) Synthesis of full-visible-spectrum luminescent silicon nanocrystals and the origin of the luminescence. Appl Phys A 111:501–507
63. Erogbogbo F, Yong KT, Roy I, Xu GX, Prasad PN, Swihart MT (2008) Biocompatible luminescent silicon quantum dots for imaging of cancer cells. ACS Nano 2(5):873–878
64. Shen P, Ohta S, Inasawa S, Yamaguchi Y (2011) Selective labeling of the endoplasmic reticulum in live cells with silicon quantum dots. Chem Commun (Camb) 47:8409–8411
65. Zhong Y, Peng F, Bao F, Wang S, Ji X, Yang L, Su Y, Lee ST, He Y (2013) Large-scale aqueous synthesis of fluorescent and biocompatible silicon nanoparticles and their use as highly photostable biological probes. J Am Chem Soc 135:8350–8356
66. Wu J, Dai J, Shao Y, Sun Y (2015) One-step synthesis of fluorescent silicon quantum dots (Si-QDs) and their application for cell imaging. RSC Adv 5:83581–83587
67. Erogbogbo F, Chang CW, May J, Prasad PN, Swihart MT (2012) Energy transfer from a dye donor to enhance the luminescence of silicon quantum dots. Nanoscale 4:5163–5168
68. Tu CQ, Ma XC, Pantazis P, Kauzlarich SM, Louie AY (2010) Paramagnetic, silicon quantum dots for magnetic resonance and two-photon imaging of macrophages. J Am Chem Soc 132:2016–2023
69. Stan MS, Sima C, Cinteza LO, Dinischiotu A (2015) Silicon-based quantum dots induce inflammation in human lung cells and disrupt extracellular matrix homeostasis. FEBS J 282:2914–2929
70. Stan MS, Memet I, Sima C, Popescu T, Teodorescu VS, Hermenean A, Dinischiotu A (2014) Si/SiO_2 quantum dots cause cytotoxicity in lung cells through redox homeostasis imbalance. Chem Biol Interact 220:102–115
71. Stanca L, Sima C, Petrache Voicu SN, Serban AI, Dinischiotu A (2015) In vitro evaluation of the morphological and biochemical changes induced by Si/SiO_2 QDs exposure of HepG2 cells. Rom Rep Phys 67:1512–1524
72. De Stefano D, Carnuccio R, Maiuri MC (2012) Nanomaterials toxicity and cell death modalities. J Drug Deliv. Article ID 167896
73. Shiohara A, Hanada S, Prabakar S, Fujioka K, Lim TH, Yamamoto K, Northcote PT, Tilley RD (2010) Chemical reactions on surface molecules attached to silicon quantum dots. J Am Chem Soc 132:248–253
74. Stern ST, Zolnik BS, McLeland CB, Clogston J, Zheng J, McNeil SE (2008) Induction of autophagy in porcine kidney cells by quantum dots: a common cellular response to nanomaterials? Toxicol Sci 106:140–152
75. Luo YH, Wu SB, Wei YH, Chen YC, Tsai MH, Hp CC, Lin SY, Yang CS, Lin P (2013) Cadmium-based quantum dot induced autophagy formation for cell survival via oxidative stress. Chem Res Toxicol 26:662–673
76. Stern ST, Adiseshaiah PP, Crist RM (2012) Autophagy and lysosomal dysfunction as emerging mechanisms of nanomaterial toxicity. Part Fibre Toxicol 9:20
77. Tu C, Ma X, House A, Kauzlarich SM, Louie AY (2011) PET imaging and biodistribution od silicon quantum dots in mice. ACS Med Chem Lett 2:285–288
78. Liu J, Erogbogbo F, Yong KT, Ye L, Liu J, Hu R, Chen H, Hu Y, Yang Y, Yang J, Roy I, Karker NA, Swihart MT, Prasad PN (2013) Assessing clinical prospects of silicon quantum dots: studies in mice and monkeys. ACS Nano 7:7303–7310
79. Erogbogbo F, Yong KT, Roy I, Hu R, Law WC, Zhao W, Ding H, Wu F, Kumar R, Swihart MT, Prasad PN (2011) In vivo targeted cancer imaging, sentinel lymph node mapping and multi-channel imaging with biocompatible silicon nanocrystals. ACS Nano 5:413–423
80. Stanca L, Petrache SN, Serban AI, Staicu AC, Sima C, Munteanu MC, Zărnescu O, Dinu D, Dinischiotu A (2013) Interaction of silicon-based quantum dots with gibel carp liver: oxidative and structural modifications. Nanoscale Res Lett 8:254
81. Serban AI, Stanca L, Sima C, Staicu AC, Zarnescu O, Dinischiotu A (2015) Complex responses to Si quantum dots accumulation in carp liver tissue: beyond oxidative stress. Chem Biol Interact 239:56–66

82. Petrache SN, Stanca L, Serban AI, Sima C, Staicu AC, Munteanu MC, Costache M, Burlacu R, Zarnescu O, Dinischiotu A (2012) Structural and oxidative changes in the kidney of crucian carp induced by silicon-based quantum dots. Int J Mol Sci 13:10193–101211
83. Stanca L, Petrache SN, Radu M, Serban AI, Munteanu MC, Teodorescu D, Staicu AC, Sima C, Costache M, Grigoriu C, Zarnescu O, Dinischiotu A (2012) Impact of silicon-based quantum dots on the antioxidative system in white muscle of Carassius auratus gibelio. Fish Physiol Biochem 38:963–975
84. Alsharif NH, Berger CEM, Varanasi SS, Chao Y, Horrocks BR, Datta HK (2009) Alkyl-capped silicon nanocrystals lack cytotoxicity and have enhanced intracellular accumulation in malignant cells via cholesterol-dependent endocytosis. Small 5:221–228
85. Ohta S, Yamura K, Inasawa S, Yamaguchi Y (2015) Aggregates of silicon quantum dots as a drug carrier: selective intracellular drug release based on pH-responsive aggregation/dispersion. Chem Commun 51:6422–6425
86. Li ZF, Ruckenstein E (2004) Water-soluble poly(acrylic acid) grafted luminescent silicon nanoparticles and their use as fluorescent biological staining labels. Nano Lett 4:1463–1467
87. Erogbogbo F, Yong KT, Hu R, Law WC, Ding H, Chang CW, Prasad PN, Swihart MT (2010) Biocompatible magnetofluorescent probes: luminescent silicon quantum dots coupled with superparamagnetic iron (III) oxide. ACS Nano 4:5131–5138
88. Erogbogbo F, Chang CW, May JL, Liu L, Kumar R, Law WC, Ding H, Yong KT, Roy I, Sheshadri M, Swihart MT, Prasad PN (2012) Bioconjugation of luminescent silicon quantum dots to gadolinium ions for bioimaging applications. Nanoscale 4:5483–5489
89. Klein S, Zolk O, Fromm MF, Schrodl F, Neuhuber W, Kryschi C (2009) Functionalized silicon quantum dots tailored for targeted siRNA delivery. Bioch Biophys Res Commun 387:164–168
90. May JL, Erogbogbo F, Yong KT, Ding H, Law WC, Swihart MT, Prasad PN (2012) Enhancing silicon quantum dot uptake by pancreatic cancer cells via pluronic® encapsulation and antibody targeting. J Solid Tumors 2:24–37
91. Erogbogbo F, Liu X, May JL, Narain A, Gladding P, Swihart MT, Prasad PN (2013) Plasmonic gold and luminescent silicon nanoplatforms for multimode imaging of cancer cells. Integr Biol 5:144–150
92. Hanada S, Fujioka K, Futamura Y, Manabe N, Hoshino A, Yamamoto K (2013) Evaluation of anti-inflammatory drug-conjugated silicon quantum dots: their cytotoxicity and biological effect. Int J Mol Sci 14:1323–1334
93. Paul A, Jana A, Karthik S, Bera M, Zhao Y, Singh NDP (2016) Photoresponsive real time monitoring silicon quantum dots for regulated delivery of anticancer drugs. J Mater Chem B 4:521–528
94. Erogbogbo F, May J, Swihart M, Prasad PN, Smart K, Jack SE, Korcyk D, Webster M, Stewart R, Zeng I, Jullig M, Bakeev K, Jamieson M, Kasabov N, Gopalan B, Liang L, Hu R, Schliebs S, Villas-Boas S, Gladding P (2013) Bioengineering silicon quantum dot theranostics using a network analysis of metabolomic and proteomic data in cardiac ischemia. Theranostics 3:719–728
95. Olson JL, Velez-Montoya R, Mandava N, Stoldt CR (2012) Intravitreal silicon-based quantum dots as neuroprotective factors in a model of retinal photoreceptor degeneration. Invest Ophthalmol Vis Sci 53:5713–5721